Journal of Medical and Biological Engineering (2022) 42:780–789
https://doi.org/10.1007/s40846-022-00763-y

ORIGINAL ARTICLE

Radiomics of Multi-modality Ultrasound in Rabbit VX2 Liver Tumors: Differentiating Residual Tumors from Hyperemic Rim After Ablation

Yucai Dong[1,2,3] · Qi Zhang[1,3] · Haobo Chen[1,3] · Yunjie Jin[4,5] · Zhengbiao Ji[4,5] · Hong Han[4,5] · Wenping Wang[4,5]

Received: 21 July 2022 / Accepted: 2 November 2022 / Published online: 17 November 2022

Abstract

Purpose To investigate the value of quantitative features extracted from multi-modality ultrasound, composed of B-mode ultrasound (BUS), strain elastography (SE), and contrast-enhanced ultrasound (CEUS), in the early differentiation of residual tumors from hyperemic rim after ablation for rabbit VX2 liver tumors.

Methods The study included sixteen rabbits undergoing ablation for normal liver tissue or VX2 liver tumors. BUS, SE, and CEUS examinations of rabbit livers were performed on day 3 and day 7 after ablation. A total of 108 radiomics features were extracted. Spearman rank correlation, the t-test, Kruskal-Wallis test (KW-test), and the least absolute shrinkage and selection operator (LASSO) method were applied to analyze data. The support vector machine (SVM) and logistic regression (LR) classifiers were used to classify hyperemic rim and residual tumors under the leave-one-out cross-validation. Model performance was validated by the area under the receiver operating characteristic curve (AUC).

Results All ultrasound modalities had features that significantly differed between hyperemic rim and residual tumors, such as the maximal value of BUS, the entropy of brightness of SE, and the skewness value of CEUS (all $p < 0.05$). For the differentiation between hyperemic rim and residual tumors after ablation, the AUC of multi-modality ultrasound was 93.3% on day 3 and 82.1% on day 7.

Conclusion The multi-modality ultrasound radiomics is helpful for the early differentiation between hyperemic rim and residual tumors around the ablation area in a rabbit model, which might improve future ablation for liver tumors.

Keywords Multi-modality ultrasound · Radiomics · Ablation · Liver tumor

1 Introduction

Radiofrequency (RF) ablation has become an important method for treating hepatic malignancies due to less trauma and quick recovery [1–3]. However, incomplete ablation due to tumor proximity to important structures, such as blood vessels and diaphragm, or operator technical problems, results in residual tumors. Accurate early postoperative follow-up strategies are crucial for improving survival [4]. Although, it is often difficult to assess the effects of RF ablation by early postoperative imaging. An ablation-induced hyperemic rim appears in the ablated zone, known as benign periablational enhancement (BPE) [5]. The BPE remains for a long time, even up to six months, and it is often mistaken for the residual tumor, which is also characterized by periablational enhancement on imaging [6].

✉ Qi Zhang
zhangq@t.shu.edu.cn

✉ Hong Han
han.hong@zs-hospital.sh.cn

✉ Wenping Wang
wang.wenping@zs-hospital.sh.cn

1 Shanghai Institute for Advanced Communication and Data Science, The SMART (Smart Medicine and AI-based Radiology Technology) Lab, Shanghai University, Shanghai 200444, China

2 Suzhou Institute of Biomedical Engineering,Technology Chinese Academy of Sciences, Suzhou 215163, China

3 School of Communication and Information Engineering, Shanghai University, Shanghai 200444, China

4 Department of Ultrasound, Zhongshan Hospital, Fudan University, Shanghai 200032, China

5 Shanghai Institute of Medical Imaging, Shanghai 200032, China

Ultrasound imaging with high spatial resolution plays a crucial role in postoperative follow-up because low-cost and safety of ultrasound imaging allows repeated real-time dynamic observations. However, BPE is difficult to distinguish from residual tumor on conventional ultrasound. The residual tumor is characterized by periablational enhancement on contrast-enhanced ultrasound (CEUS) scan. Computed tomography (CT) and magnetic resonance imaging (MRI) can also be used for post-ablation assessment. However, early differentiation between BPE and residual tumors remains a major problem even after using contrast-enhanced CT and contrast-enhanced MRI. This issue can seriously affect subsequent clinical decisions making [7–9]; therefore, a new method is urgently needed for early differentiation between BPE and residual cancer to help physicians' judgment.

Radiomics is a computer-aided radiological technology that uses high-throughput characteristics of medical images to identify diseases, assess therapeutic efficacy, and predict prognosis [10–13]. Multi-modal ultrasound technology combines two or more ultrasound methods for multi-angle analysis and improves diagnosis accuracy. Currently, B-mode ultrasound (BUS), strain elastography (SE), and CEUS are the three most commonly used modes of ultrasound imaging after RF ablation. BUS can provide valuable information about the liver lesion, including its size, shape, margins, and internal echo [14]. SE reflects the elasticity of liver tissue [15]. CEUS uses a contrast agent to enhance the backscattered echoes from the blood perfusion of normal and abnormal liver tissues [16, 17]. The application of multi-modal ultrasound technology can integrate the information from BUS, SE, and CEUS to improve the accuracy of diagnosis [18].

Previously, Vilana et al. [19] used microbubble-enhanced ultrasonography to evaluate residual cancer on day 1 after ablation and found that the sensitivity was only 27.3%. Yi et al. [20, 21] investigated the value of the perfusion parameters of CEUS in the early differentiation between BPE and residual tumors after ablation. Hong et al. [22] assessed shear wave dispersion imaging parameters at different time points after ablation. Previous studies were based on only one modality of ultrasound, and our study is the first one to combine BUS, SE, and CEUS in the analysis of post-ablation liver cancer. In addition, we extracted new high-throughput features by radiomics. There are few studies using radiomics for distinguishing BPE from residual cancer after ablation.

In this study, we used a rabbit VX2 liver tumor model for early differentiation between residual tumors and hyperemic rim after ablation. Since animal experiments can easily provide tissue specimens for pathological assessment, residual tumors, coagulation areas, and BPE can be accurately detected. The radiomics of multi-modality ultrasound, including BUS, SE, and CEUS, was investigated in this study. It assisted early post-ablation differentiation between these two conditions in an animal model; therefore, necessary therapeutic actions can be decided as soon as possible. Furthermore, this study also provides an experimental basis for the early identification of residual tumors after ablation in clinics.

2 Materials and Methods

2.1 Animal Models and Ultrasonic Imaging

The flowchart of this study is shown in Fig. 1. The experimental protocols were approved by the Institutional Animal Care and Use Committee at the authors' institution. The experiments were performed with sixteen New Zealand white rabbits weighing 2.5–3.0 kg. VX2 carcinoma was inoculated in the livers of thirteen rabbits with a well-established method. Two weeks later, the tumors were used for laser ablation, and the maximum tumor diameters ranged from 1.1 to 1.3 cm. We then built a partially ablated tumor model by using laser ablation technology. Under ultrasound guidance, the 21-gauge PTC needle was inserted directly into tumor position. The needle core was removed, and the laser fiber (diameter, 300 μm; wavelength, 1064 nm) was pushed forward with 5 mm of its tip exposed. The ablation power was set at 4 W, and burning continued until the action energy reached 100 J. The size of the ablation was about 1/3 – 2/3 of the tumor. The fully ablated side was surrounded by a hyperemic rim, and the residual tumor was in the partially ablated zone (Fig. 2). In the other three rabbits, we did not implant the tumor and only ablated their normal liver tissue to test the formation of BPE. The ablation procedure and instruments were the same for normal liver tissue and tumor. In total, there were sixteen zones of BPE and thirteen zones of residual tumors.

BUS, SE, and CEUS were performed on rabbit models on day 3 and day 7 after ablation. The instruments were Resona 8 (Mindray, Shenzhen, China), and Aplio i900 (Canon, Tochigi-ken, Japan) color Doppler ultrasound apparatuses.

To measure the consistency between imaging and histopathology, the VX2 rabbits were randomly sacrificed 3 or 7 days after ablation. The specimen [23] corresponding to the ultrasound image was cut from the center of the ablation lesion, including the residual tumor, ablation coagulation lesion, hyperemic rim zone, and normal liver tissue (Fig. 2a). Then the specimen was fixed in 10% neutral formalin solution and subsequently stained with hematoxylin and eosin for histopathological measurement [24]. Each section (Fig. 2b) was carefully examined by an expert pathologist, and all findings were recorded.

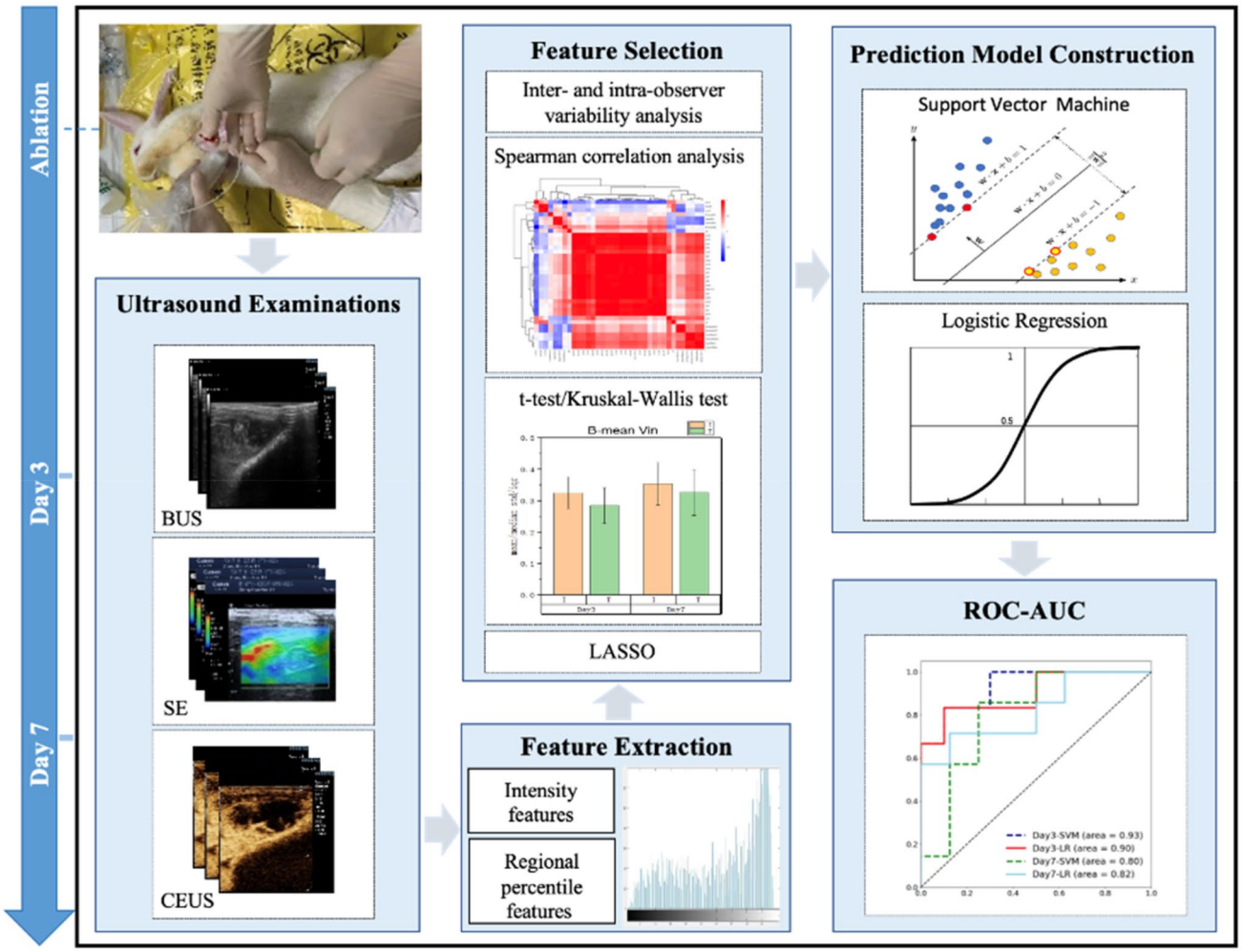

Fig. 1 The flow chart of the radiomics method for differentiation of the residual cancer and the inflammatory reaction after ablation. Firstly, A rabbit model of partial ablation of liver tumors was constructed. Secondly, BUS, SE and CEUS examinations were performed on day 3 and day 7 after ablation. Radiomics features were extracted. Then, a four-stage process was applied for feature selection. Finally, prediction models were constructed with the support vector machine and logistic regression classifiers, evaluated with ROC

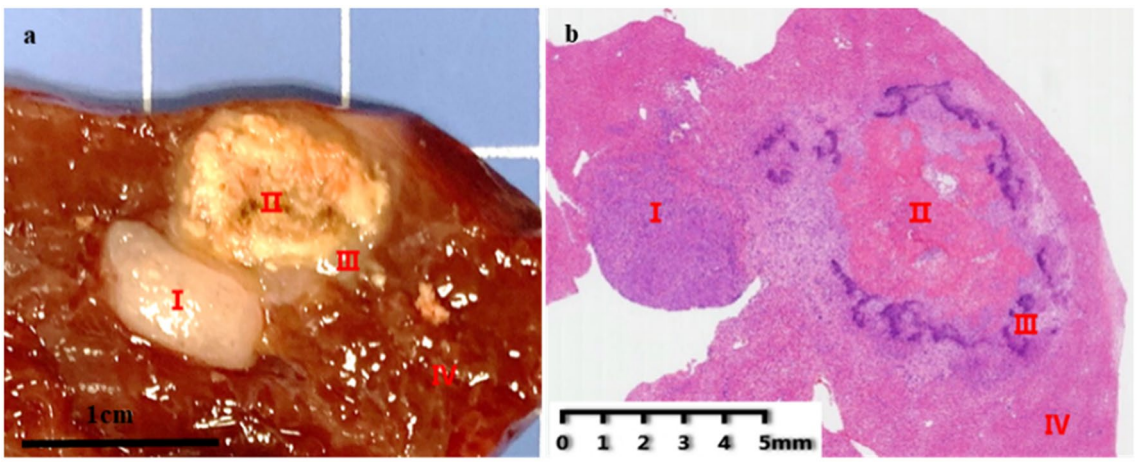

Fig. 2 A rabbit model of partial ablation of liver tumors. **a** The gross specimen of an incompletely ablated tumor; **b** The corresponding pathological specimen of the incompletely ablated tumor. Four areas are denoted, namely the residual tumors (I), coagulation areas (II), benign periablational enhancement (BPE, III) and normal liver tissue (IV)

2.2 Image Preprocessing

Multi-modality ultrasound and pathological images are shown in Fig. 3. The margins of BPE and tumoral zones were determined with red curves by a radiologist with 10 years of experience. Two months later, the same radiologist determined the lesion contours of 10 random rabbits to assess intraclass correlation coefficients (ICCs). As shown in Fig. 4, image preprocessing was performed on three modalities. The regions inside the boundaries were filled to get the binary masks of BPE (Fig. 4a) and tumoral (Fig. 4c) zones. In addition, for the SE images (Fig. 4b), the pure elasticity map was derived from the difference between the region of interest (ROI) in a color elastogram and that in a grayscale B-mode image. The color bar on the left of Fig. 4b shows the elasticity of the tissue, and the color spectrum from red to blue indicates the elasticity from soft to hard. According to the color bar, the pure elasticity map was transformed into the grayscale softness map ranging from 0 (the hardest) to 1 (the softest) [25].

2.3 Multi-Modality Feature Extraction

In this study, the radiomics feature extraction was performed with MATLAB. Before the feature extraction, we grayed and normalized the softness map or ultrasonic image. A total of 108 radiomics features, including 36 for each modality with intensity features and regional percentile features, were extracted from BUS, SE and CEUS images. The image intensity features included the mean value (meanV), standard deviation value (stdV), coefficient of variation (CoV), skewness value (skewV), entropy of brightness (EntropyBrt), entropy of histogram (EntropyHis), mean region of interest (meanROI), median region of interest (medianROI), mean ratio (meanRatio), and median ratio (medianRatio) [26]. qx indicates regional percentile features, and x (ranging from 0 to 1 at a step of 0.05) indicates the percentage of the queue relative to the whole pixel queue. q*x* indicates the pixel value, q0 and q1 indicate the minimum value (minV) and the maximum value (maxV), respectively.

2.4 Feature Selection

In order to prevent models from overfitting, feature selection was performed. We used a four-step procedure to select radiomic features. First, z-score standardization and normalization were applied to radiomic features. Then, ICCs were calculated (ICCs > 0.75 indicated good reproducibility). In the second stage, spearman correlation analysis was used to select features. A pairwise Spearman correlation coefficients (defined as r_s) matrix was calculated, and $|r_s| > 0.9$ were identified as highly correlated. For each highly correlated

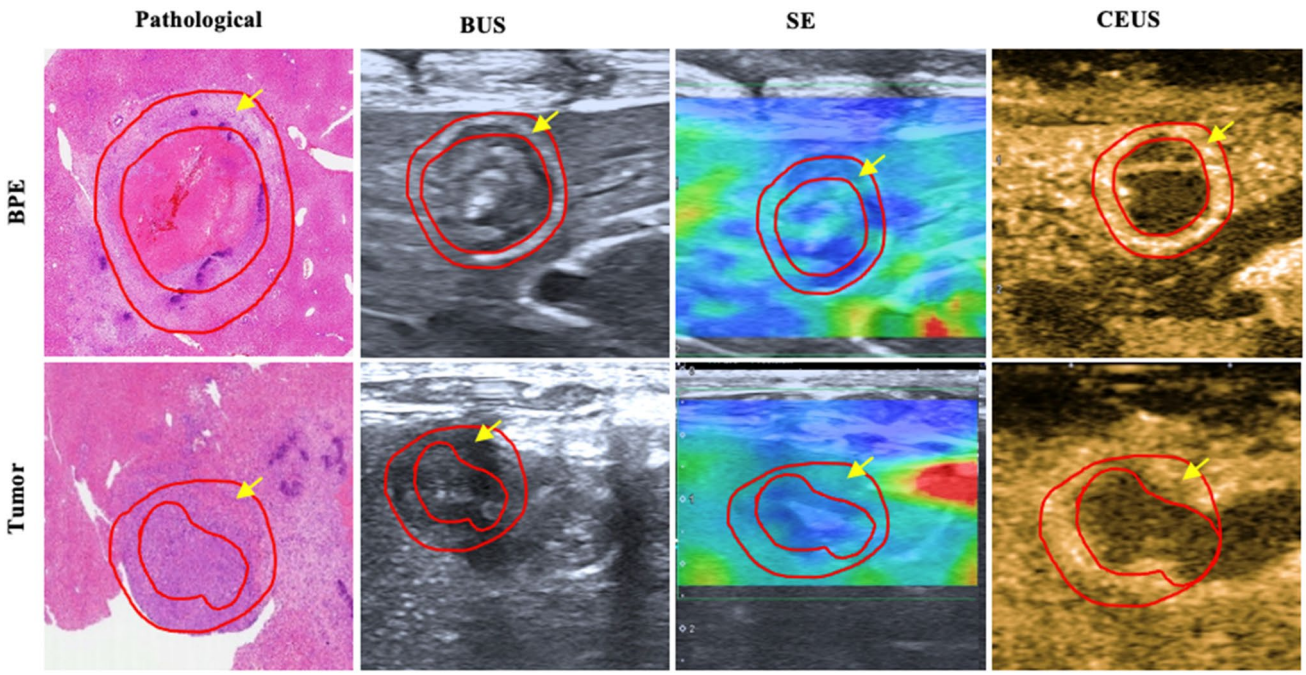

Fig. 3 Multi-modality ultrasound images and pathological images of benign periablational enhancement (BPE) and residual tumors after ablation. The middle ring areas surrounded by two red circles (pointed by yellow arrows) are BPE and peripheral residual tumor regions. They are all characterized by enhancement around the ablation focus on imaging examinations. It is difficult to early distinguish between BPE and residual tumors by BUS, SE or CEUS after ablation

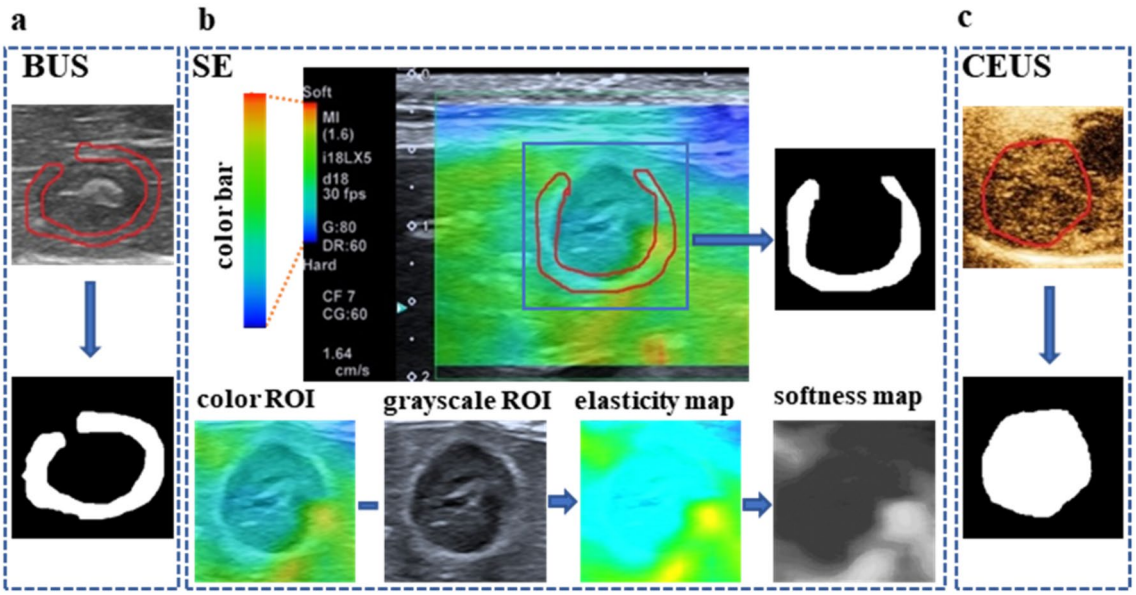

Fig. 4 The image preprocessing of BUS, SE and CEUS. **a** The image preprocessing for BUS of an inflammatory reaction, where the binary mask was derived by filling the delineated boundary (red), **b** The image preprocessing for SE of an inflammatory reaction, where the softness map was derived from the elasticity map according to the color bar, **c** The image preprocessing of CEUS of a residual cancer

feature pair, only the one feature with the lower average $|r_s|$ between a feature and all the other features was considered to be retained [27]. In the third stage, the t-test was used for variables with normal distribution, and the Kruskal-Wallis test (KW-test) was used for variables without normal distribution to compare the inflammation group with the tumor group. Then ten first-stage selected features with the minimum p values were identified to be used in the fourth stage. At the final stage, the least absolute shrinkage and selection operator (LASSO) feature selection algorithm was used to detect important features under the leave-one-out cross-validation. We determined the intersection features of all models with important features as the final features under the leave-one-out cross-validation. Finally, two features were selected for each case.

2.5 Prediction Model Construction

The construction and evaluation of classification models were performed using Python, version 3.6. The support vector machine (SVM) [28] and logistic regression (LR) classifiers, which are suitable for a small sample dataset, were adopted to construct the radiomics model in this study [29]. We used three single-modality feature datasets and one multi-modality feature dataset to construct models. The single-modality models were constructed based on the optimal feature subsets obtained by feature selection. The SVM classification score for each single-modality model was calculated as a new feature. Similar to multi-modality model, we incorporated single-modality optimal feature subsets and the SVM scores; therefore, each modality had three optional features. Then, we took one feature from each modality to produce a three-feature combination for the multi-modality model. Thus, 27 combinations of multi-modality features were built to establish the multi-modality models under the leave-one-out cross-validation, and the model with the optimal area under the receiver operating characteristic curve (AUC) value was selected as the final multi-modality model.

The receiver operating characteristic (ROC) curves were used to evaluate the classification results. The accuracy (ACC), sensitivity (SEN), specificity (SPE), AUC, and standard error of AUC were calculated, taking the maximum Youden's index as the optimal critical point.

2.6 Statistical Analysis

After partial ablation of liver tumors, statistical analysis was performed to compare the characteristics of different regions. First, normal distribution and homogeneity of variances were tested for radiomic features. For features with satisfying normal distribution and homogeneity of variance, we used the t-test to select features with significant differences ($p < 0.05$) and calculated the mean and standard deviation (STD). For features without satisfying normal distribution or homogeneity of variances, we used KW-test to select features ($p < 0.05$) and calculated the median and interquartile range (IQR).

3 Results

3.1 Statistically Significant Features from BUS, SE and CEUS Images

The statistics of BUS, SE, and CEUS features on day 3 and day 7 after ablation are shown in Table 1. BUS features, namely stdV, q0.6, q0.8, q0.9, and maxV, showed significant differences between the BPE and tumor groups on day 3 ($p < 0.05$), and EntropyHis exhibited a significant difference on day 7 ($p = 0.044$). SE features, including CoV, EntropyBrt, and q0.45, showed significant differences on day 7 ($p < 0.05$). On day 3, there were significant differences in CEUS features, including meanV, skewV, q0.5, q0.95, meanROI, medianROI, meanRatio, and medianRatio (all $p < 0.01$ except for skewV with $p = 0.018$).

3.2 Diagnostic Performance in BPE and Residual Tumors

The classification performance is shown in Table 2. The corresponding ROC curves are shown in Fig. 5. The classification results on BUS indicated that the maximum AUC and ACC were 74.4% and 80.8% on day 3, and 77.5% and 77.8% on day 7. The SPEs ranged from 80.0 to 93.8% at two time points, and SENs were between 60.0% and 75.0%.

The classification results on SE showed that the largest AUC and ACC were 58.3% and 63.2% on day 3 and 72.2% and 84.2% on day 7, respectively. The SENs were 71.4% on day 3 and 66.7% on day 7, while the SPEs were between 58.3% and 100.0%.

The classification results on CEUS indicated that the largest AUC was 84.6% on day 3 and 75.0% on day 7. The SENs with two classifiers were 71.4% on day 3, and 100.0% and 85.7% on day 7. SPEs were 92.3% on day 3, and 50.0% and 62.5% on day 7.

The classification results indicated that on day 3, the multi-modality model with the SVM classifier (AUC = 93.3%) was superior to the SE model (AUC = 58.3%, Delong test: $Z = 2.203$, $p = 0.028$). On day 7, the multi-modality model had an AUC of 82.1%, with no significant improvement compared with the AUC of single-modality models (Delong test: $p > 0.05$). The SENs with the SVM and LR classifiers were 83.3% on day 3 and between 71.4% and 85.7% on day 7. SPEs ranged from 75.0 to 90.0%.

4 Discussion

Recently, radiomics emerged as an effective method for deep mining of disease information combined with medical imaging. It can reflect abnormal tissue alterations [30, 31]. Furthermore, multi-modal ultrasound technology can integrate information from different modalities to improve computer-aided performance. The differentiation between BPE and residual cancer is difficult on imaging. We used radiomics of multi-modality ultrasound

Table 1 BUS, SE and CEUS features in the inflammation group and the tumor group on day 3 and day 7 after ablation

Modality	Feature	Day 3			Day 7		
			Inflammation	Tumor		Inflammation	Tumor
		p	Mean ± STD / Median (IQR)	Mean ± STD / Median (IQR)	p	Mean ± STD / Median (IQR)	Mean ± STD / Median (IQR)
BUS	stdV	**0.031**	0.112(0.020)	0.087(0.040)	0.063	0.139 ± 0.023	0.112 ± 0.035
	EntropyHis	0.070	6.489 ± 0.337	6.248 ± 0.274	**0.044**	6.880 ± 0.322	6.481 ± 0.453
	q0.6	**0.047**	0.332 ± 0.052	0.288 ± 0.053	0.267	0.374 ± 0.074	0.333 ± 0.076
	q0.8	**0.023**	0.395 ± 0.060	0.338 ± 0.055	0.155	0.466 ± 0.092	0.403 ± 0.082
	q0.9	**0.033**	0.456 ± 0.068	0.392 ± 0.073	0.186	0.537 ± 0.100	0.472 ± 0.101
	maxV	**0.022**	0.860(0.080)	0.748(0.227)	0.594	0.859(0.016)	0.818(0.168)
SE	CoV	0.315	0.411 ± 0.191	0.331 ± 0.086	**0.042**	0.467 ± 0.231	0.260 ± 0.171
	EntropyBrt	0.769	0.971 ± 0.025	0.974 ± 0.020	**0.034**	0.979(0.014)	0.988(0.008)
	q0.45	0.731	0.239(0.063)	0.243(0.117)	**0.049**	0.224 ± 0.069	0.365 ± 0.198
CEUS	meanV	**0.004**	0.493 ± 0.086	0.366 ± 0.069	0.632	0.498 ± 0.144	0.464 ± 0.128
	skewV	**0.018**	0.283 ± 0.317	0.091 ± 0.289	0.629	0.367 ± 0.776	0.203 ± 0.422
	q0.5	**0.004**	0.511 ± 0.106	0.361 ± 0.078	0.634	0.515 ± 0.171	0.474 ± 0.152
	q0.95	**0.003**	0.751 ± 0.095	0.600 ± 0.092	0.517	0.735 ± 0.112	0.694 ± 0.132
	meanROI	**0.004**	0.268 ± 0.078	0.378 ± 0.060	0.226	0.291 ± 0.071	0.337 ± 0.069
	medianROI	**0.001**	0.219 ± 0.095	0.384 ± 0.077	0.207	0.237 ± 0.092	0.301 ± 0.093
	meanRatio	**< 0.001**	2.033 ± 0.427	0.979 ± 0.184	0.102	1.826 ± 0.463	1.456 ± 0.326
	medianRatio	**< 0.001**	2.263(1.997)	0.926(0.216)	0.277	2.390 ± 0.756	1.889 ± 0.957

The p-values less than 0.05 are denoted in a bold font

Table 2 The leave-one-out cross validation results for discriminating between the tumor group and inflammation group when using selected radiomic features of BUS, SE and CEUS, respectively, as well as a three-feature combination of multi-modality ultrasound. The cognitive indexes include accuracy (ACC), sensitivity (SEN), specificity (SPE), area under the receiver operating characteristic curve (AUC) and standard error of AUC.

Modality	Day	Classifier	ACC (%)	SEN (%)	SPE (%)	AUC (%)	Standard Error (%)
BUS	Day 3	SVM	80.8	60.0	93.8	74.4	12.0
		LR	80.8	60.0	93.8	73.1	12.0
	Day 7	SVM	77.8	75.0	80.0	77.5	11.5
		LR	77.8	75.0	80.0	73.8	12.6
SE	Day 3	SVM	63.2	71.4	58.3	58.3	14.6
		LR	63.2	71.4	58.3	56.0	16.0
	Day 7	SVM	84.2	66.7	100.0	72.2	14.4
		LR	73.7	66.7	80.0	64.4	15.3
CEUS	Day 3	SVM	85.0	71.4	92.3	84.6	9.4
		LR	85.0	71.4	92.3	84.6	9.2
	Day 7	SVM	73.3	100.0	50.0	75.0	14.0
		LR	73.3	85.7	62.5	69.6	14.9
Muti-modality	Day 3	SVM	87.5	83.3	90.0	93.3	6.2
		LR	87.5	83.3	90.0	93.3	6.2
	Day 7	SVM	80.0	85.7	75.0	80.4	12.3
		LR	80.0	71.4	87.5	82.1	11.7

to differentiate them after ablation in the rabbit VX2 liver tumor model. Radiomics features were extracted, selected, and used in classification models to help clinical decision-making.

From day 3 to day 7 after ablation, local inflammatory reaction changed from acute to chronic inflammation in pathology [32, 33]. On day 3, there were significant differences in CEUS features between BPE and the tumor. The CEUS intensities were larger in BPE than in the residual tumor. It was speculated that this was related to the pathophysiologic changes in the ablated tissue. In response to thermal injury, the acute inflammatory reaction occurred in the periablational zone, characterized by reactive hyperemia, edema, and infiltration of neutrophils and macrophages. Acute hyperemia was characterized by dilated small blood vessels and a marked increase in blood flow. The acute inflammatory reaction might peak on the third day after ablation. However, the blood supply of the residual tumor and microvessel density decreased. Therefore, quantitative parameters related to blood flow were sensitive indicators for differentiating between residual tumor and BPE on day 3.

After 7 days of ablation, the radiomics features of BUS (stdV and EntropyHis) and SE (Cov and EntropyBrt) indicated that the uniformity of the lesion was lower in the BPE than in the residual tumor. This may be because BPE around the ablation focus manifested as the chronic inflammatory response from day 7 after ablation. Acute reactive hyperemia gradually decreased and was replaced by chronic inflammation, granulation tissue, and fibrosis. Thus, the quantitative features of BUS and SE related to uniformity were sensitive indicators for differentiating between periablational inflammatory rim and residual tumor on day 7.

Radiomics is an important method for the holistic analysis of diseases and can reveal subtle pathological changes in tissue and promote the diagnosis, treatment, and prognosis [34]. In the early stage, BPE and residual tumors are not discernible by simple multi-modality ultrasound; however, they can be distinguished by some features, such as blood flow and tissue homogeneity. In addition, our classification results showed that AUC and ACC of multi-modality ultrasound were 93.3% and 87.5% on day 3 and 82.1% and 80.0% on day 7, much higher than that on single-modality ultrasound. Furthermore, the SENs and SPEs of multi-modality ultrasound models were more balanced than those of single-modality ultrasound modes. Thus, radiomics of multi-modality ultrasound serves as a more efficient method in the early identification of BPE and residual tumors compared with single-modality ultrasound modes.

Han et al. [35] reported that on day 3 after ablation, the difference between BPE and residual tumors was most significant, confirming our hypothesis. Kan et al. [36] showed that even a stress test of CEUS with phenylephrine, could barely differentiate BPE from the residual tumor on day 7. However, we found that pathological tissue uniformity features extracted from BUS and SE can significantly differentiate between BPE and residual tumors. Of course, our study had some limitations. First, despite similarities, there are differences between BPE and residual tumors in our animal model and in human studies. Similarly, there are some pathological differences between VX2 tumor and human hepatoma. Therefore, the methods in this animal study need to be validated in human studies. Second, the small sample size limits the generalizability of our findings, and more cases are needed to validate the effectiveness of

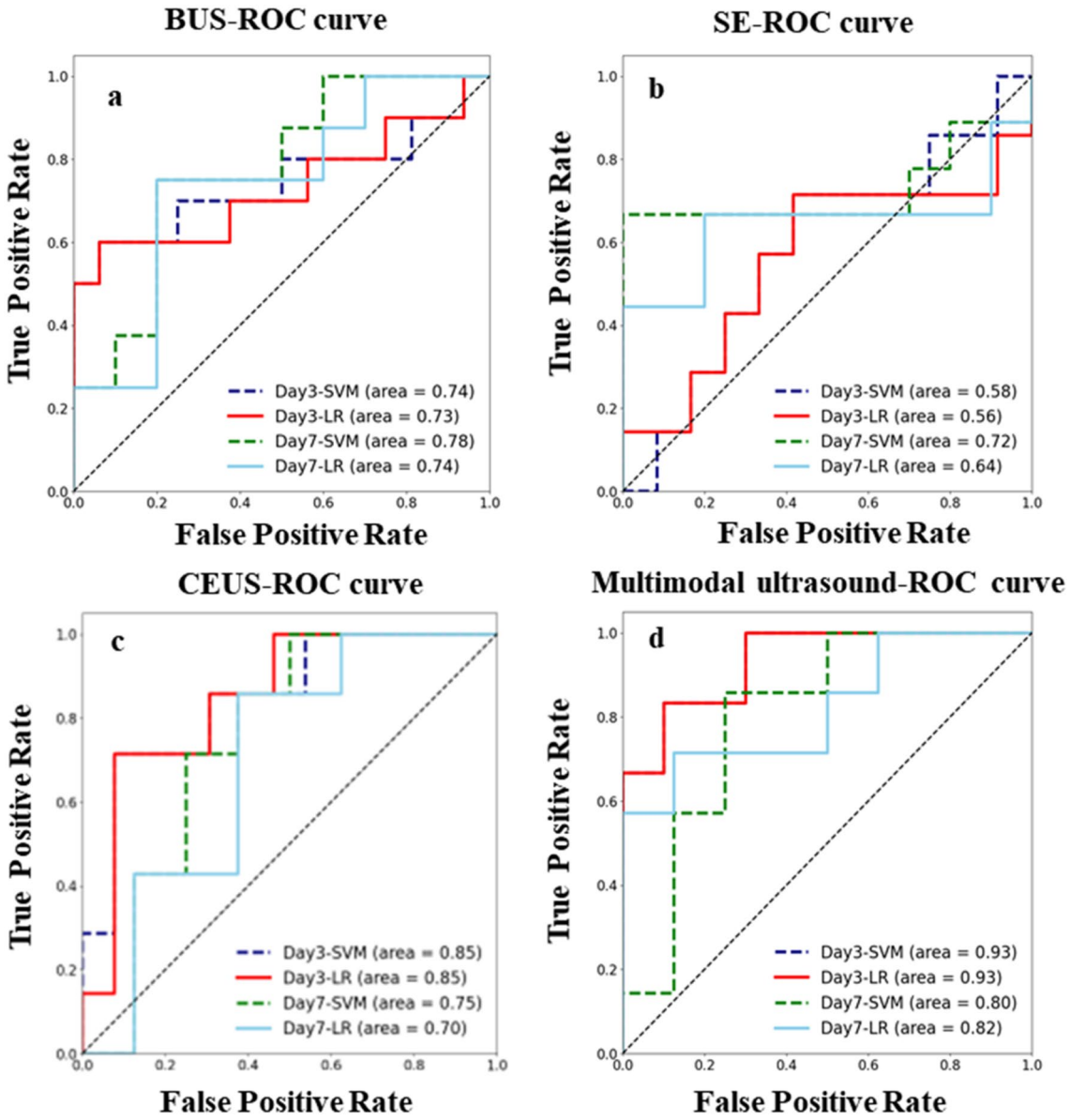

Fig. 5 ROC curves for discrimination between inflammatory reaction and residual tumors in BUS, SE, CEUS and multimodality ultrasound **a** ROC curves of BUS, **b** ROC curves of SE, **c** ROC curves of CEUS, **d** ROC curves of multimodality ultrasound

multi-modality ultrasound radiomics. Furthermore, more quantitative features, such as those derived from deep learning algorithms, can be used in the radiomics approaches to assist in early discrimination between BPE and residual tumor.

5 Conclusion

In summary, the accurate identification of BPE and residual tumors after ablation is crucial for clinical decision-making. However, the inflammatory area around the lesion is often undistinguishable from residual tumors even within 6 months after ablation, which has always been a critical problem in clinical practice. In this study, the AUC of the multimodal ultrasound model was as high as 93.3% on day 3 after ablation, indicating that it is a feasible method for early differentiation of residual tumors from BPE. Our study demonstrated that multi-modality ultrasound alterations are consistent with the pathological changes after ablation in rabbit VX2 liver tumors. It can help understand the pathological changes induced by ablation. The techniques of multi-modality ultrasound radiomics could be used in clinical settings to facilitate the early assessment of therapeutic response.

Supplementary Information The online version contains supplementary material available at https://doi.org/10.1007/s40846-022-00763-y.

Author Contributions All authors contributed to the study conception and design. YJ, ZJ, HH and WW: Material preparation and data collection were performed. YD, QZ and HC: designed the studies. YD, QZ and HH: drafted and critically revised the manuscript. All authors read and approved the final manuscript.

Funding This work was supported by the National Natural Science Foundation of China (Grant No. 62071285) and Natural Science Foundation of Shanghai (grant number: 19ZR1450700).

Declarations

Conflict of interests The authors have no relevant financial or non-financial interests to disclose.

Ethical Approval All applicable institutional and/or national guidelines for the care and use of animals were followed.

Consent to Participate For this study consent to participate is not required.

Consent to Participate For this study consent for publication is not required.

References

1. Ziemlewicz, T. J., Wells, S. A., Lubner, M. G., Brace, C. L., Lee, F. T., & Hinshaw, J. L. (2016).Hepatic Tumor Ablation. Surgical Clinics. 96(2),315–339. https://doi.org/10.1016/j.suc
2. Shiina, S., Tateishi, R., Arano, T., Uchino, K., Enooku, K., Nakagawa, H., asaoka, Y., Sato, T., Masuzaki, R., Kondo, Y., Goto, T., Yoshida, H., Omata, M., & Koike, K. (2012). Radiofrequency ablation for hepatocellular carcinoma: 10-year outcome and prognostic factors. *American Journal Of Gastroenterology*, *107*(4), 569. https://doi.org/10.1038/ajg.2011.425.
3. Nakajima, K., Yamanaka, T., Nakatsuka, A., Haruyuki, T., Fujimori, M., Sugino, Y., Matsushita, N., Sakuma, H., Isaji, S., Takei, Y., & Yamakado, K. (2016). Clinical utility of radiofrequency ablation following transarterial injection of miriplatin-iodized oil suspension in small hepatocellular carcinoma. *Japanese journal of radiology, 34*(9), 640–646. https://doi.org/10.1007/s11604-016-0567-x
4. McWilliams, J. P., Yamamoto, S., Raman, S. S., Loh, C. T., Lee, E. W., Liu, D. M., & Kee, S. T. (2010). Percutaneous ablation of hepatocellular carcinoma: Current status. *Journal Of Vascular And Interventional Radiology, 21*(8), S204–S213. https://doi.org/10.1016/j.jvir.2009.11.025
5. Nahum Goldberg, S., Grassi, C. J., Cardella, J. F., Charboneau, J. W., Dodd, G. D., Dupuy, D. E., Gervais, D., Gillams, A.R., Kane, R.A., LeeJr, F.T., Livraghi, T., McGahan, J., Phillips, D.A., Rhim, H., & Silverman, S.G. (2009). Image-guided tumor ablation: Standardization of terminology and reporting criteria. *Journal of Vascular and Interventional Radiology, 20*, 377–390. https://doi.org/10.1016/j.jvir.2009.04.011
6. Clasen, S., Boss, A., Schmidt, D., Fritz, J., Schraml, C., Claussen, C. D., & Pereira, P. L. (2006). Magnetic resonance imaging for hepatic radiofrequency ablation. *European journal of radiology, 59*, 140–148. https://doi.org/10.1016/j.ejrad.2006.04.006
7. Kim, T. J., Moon, W. K., Cha, J. H., Goo, J. M., Lee, K. H., Kim, K. H., Lee, J. W., Han, J. G., Weinmann, H. J., & Chang, K. H. (2005). VX2 carcinoma in rabbits after radiofrequency ablation: Comparison of MR contrast agents for help in differentiating benign periablational enhancement from residual tumor. *Radiology, 234*, 423–430. https://doi.org/10.1148/radiol.2342031456
8. Li, Y., Shi, G., Wang, S., Wang, S., & Wu, R. (2013). Iodine quantification with dual-energy CT: Phantom study and preliminary experience with VX2 residual tumour in rabbits after radiofrequency ablation. *British Journal of Radiology*, *86*, 20130143. https://doi.org/10.1259/bjr.20130143.
9. Wu, H., Patel, R. B., Zheng, Y., Solorio, L., Krupka, T. M., Ziats, N. P., Haaga, J. R., & Exner, A. A. (2012). Differentiation of benign periablational enhancement from residual tumor following radio-frequency ablation using contrast-enhanced ultrasonography in a rat subcutaneous colon cancer model. *Ultrasound in Medicine and Biology, 38*, 443–453. https://doi.org/10.1016/j.ultrasmedbio.2011.12.008
10. Fusco, R., Granata, V., Grazzini, G., Pradella, S., Borgheresi, A., Bruno, A., Palumbo, P., Bruno, F., Grassi, R., Giovagnoni, A., & Grassi, R. (2022). Radiomics in medical imaging: pitfalls and challenges in clinical management. *Japanese Journal of Radiology*. https://doi.org/10.1007/s11604-022-01271-4
11. Cameron, A., Khalvati, F., Haider, M. A., & Wong, A. (2016). MAPS: A Quantitative Radiomics Approach for Prostate Cancer Detection. *IEEE Transactions on Biomedical Engineering*, *63*, 1145–1156. https://doi.org/10.1109/TBME.2015.2485779.
12. Zhang, Q., Xiao, Y., Suo, J., Shi, J., Yu, J., Guo, Y., Wang, Y., & Zheng, H. (2017). Sonoelastomics for breast tumor classification: A radiomics approach with clustering-based feature selection on sonoelastography. *Ultrasound in Medicine and Biology, 43*, 1058–1069. https://doi.org/10.1016/j.ultrasmedbio.2016.12.016
13. Peeken, J. C., Bernhofer, M., Wiestler, B., Goldberg, T., Cremers, D., Rost, B., Wilkens, J. J., Combs, S. E., & Nüsslin, F. (2018). Radiomics in radiooncology–challenging the medical physicist. *Physica medica, 48*, 27–36. https://doi.org/10.1016/j.ejmp.2018.03.012
14. Petzold, G., Lasser, J., Rühl, J., Bremer, S. C., Knoop, R. F., Ellenrieder, V., Kunsch, S., & Neesse, A. (2020). Diagnostic accuracy of B-Mode ultrasound and Hepatorenal Index for graduation of hepatic steatosis in patients with chronic liver disease. *PLoS One, 15*(5), e0231044. https://doi.org/10.1371/journal.pone.0231044
15. Ranjkesh, M., Hajibonabi, F., Seifar, F., Tarzamni, M. K., Moradi, B., & Khamnian, Z. (2020). Diagnostic value of elastography, strain ratio, and elasticity to B-mode ratio and color doppler ultrasonography in breast lesions. *International Journal of General Medicine*, *13*, 215. https://doi.org/10.2147/IJGM.S247980.
16. Dietrich, C. F., Nolsøe, C. P., Barr, R. G., Berzigotti, A., Burns, P. N., Cantisani, V., Chammas, M. C., Chaubal, N., Choi, B. I., Clevert, D. A., & Cui, X. (2020). Guidelines and good Clinical Practice Recommendations for Contrast-Enhanced Ultrasound (CEUS) in the liver-update 2020 WFUMB in cooperation with EFSUMB, AFSUMB, AIUM and FLAUS: WFUMB in cooperation with EFSUMB, AFSUMB, AIUM and FLAUS. *Ultrasound in Medicine and Biology, 41*, 562–585. https://doi.org/10.1016/j.ultrasmedbio.2020.04.030
17. Yao, Z., Dong, Y., Wu, G., Zhang, Q., Yang, D., Yu, J. H., & Wang, W. P. (2018). Preoperative diagnosis and prediction of hepatocellular carcinoma: Radiomics analysis based on multimodal ultrasound images. *Bmc Cancer, 18*, 1–11. https://doi.org/10.1186/s12885-018-5003-4
18. Lee, D. H., & Lee, J. M. (2018). Recent advances in the image-guided tumor ablation of liver malignancies: Radiofrequency ablation with multiple electrodes, real-time multimodality fusion imaging, and new energy sources. *In Korean Journal of Radiology*, *19*, 545–559. https://doi.org/10.3348/kjr.2018.19.4.545.

19. Vilana, R., Bianchi, L., Varela, M., et al. (2006). Is microbubble enhanced ultrasonography sufficient for assessment of response to percutaneous treatment in patients with early hepatocellular carcinoma? *European Radiology*, *16*, 2454–2462. https://doi.org/10.1007/s00330-006-0264-8.
20. Yi, H., Cai, B., Ai, X., Li, K., Song, P., & Zhang, W. (2020). Early identification of residual tumors following microwave ablation using contrast-enhanced ultrasonography in a rabbit VX2 liver cancer model. *BioMed Research International*. https://doi.org/10.1155/2020/2462058
21. Yi, H. M., Cai, B. H., Ai, X., Li, K. Y., & Zhang, W. (2019). Establishment of rabbit liver VX2 tumor model using percutaneous puncture inoculation of tumor fragment guided and evaluated by ultrasonography. *Current Medical Science, 39*(5), 820–824.
22. Han, H., Jin, Y., Liu, R., Ji, Z., Pu, M., & Wang, W. (2021). Experimental study of shear wave dispersion imaging in evaluating inflammatory reaction zone after ablation in normal rabbit liver. *Chinese Journal of Ultrasonography*, *30*(05), 441–445.
23. Gupta, S., Wallace, M. J., Cardella, J. F., Kundu, S., Miller, D. L., & Rose, S. C. (2010). Quality improvement guidelines for percutaneous needle biopsy. *Journal of vascular and interventional radiology*, *21*, 969–975. https://doi.org/10.1016/j.jvir.2010.01.011.
24. Abd Raziff, H. H., Tan, D., Tan, S. H., Wong, Y. H., Lim, K. S., Yeong, C. H., Sulaiman, N., Abdullah, B. J., Wali, H. A., Zailan, N. A., & Ahmad, H. (2021). Laser-heated needle for biopsy tract ablation: In vivo study of rabbit liver biopsy. *Physica Medica, 82*, 40–45. https://doi.org/10.1016/j.ejmp.2021.01.067
25. Zhang, Q., Cai, Y., Hua, Y., Shi, J., Wang, Y., & Wang, Y. (2017). Sonoelastography shows that Achilles tendons with insertional tendinopathy are harder than asymptomatic tendons. *Knee Surgery Sports Traumatology Arthroscopy*, *25*, 1839–1848. https://doi.org/10.1007/s00167-016-4197-8.
26. Lambin, P., Rios-Velazquez, E., Leijenaar, R., Carvalho, S., van Stiphout, R. G., Granton, P., & ML Z. C., Gillies, R., Boellard, R. Dekker, A., and Aerts, HJ,. (2012). Radiomics: Extracting more information from medical images using advanced feature analysis. *European journal of cancer, 48*, 441–446. https://doi.org/10.1016/j.ejca.2011.11.036
27. Xia, W., Hu, B., Li, H., Geng, C., Wu, Q., Yang, L., Yin, B., Gao, X., Li, Y., & Geng, D. (2021). Multiparametric-MRI-based radiomics model for differentiating primary central nervous system lymphoma from glioblastoma: Development and cross-vendor validation. *Journal of Magnetic Resonance Imaging, 53*(1), 242–250. https://doi.org/10.1002/jmri.27344
28. Fusco, R., Sansone, M., Filice, S., Carone, G., Amato, D. M., Sansone, C., & Petrillo, A. (2016). Pattern recognition approaches for breast cancer DCE-MRI classification: A systematic review. *Journal of Medical and Biological Engineering, 36*(4), 449–459.
29. Chen, W., Hua, Y., Mao, D., Wu, H., Tan, M., Ma, W., & Li, M. (2021). A Computed tomography-derived radiomics approach for predicting uncommon EGFR mutation in patients With NSCLC. *Frontiers in Oncology*. https://doi.org/10.3389/fonc.2021.722106
30. Ubaldi, L., Valenti, V., Borgese, R. F., Collura, G., Fantacci, M. E., Ferrera, G., Iacoviello, G., Abbate, B. F., Laruina, F., Tripoli, A., & Retico, A. (2021). Strategies to develop radiomics and machine learning models for lung cancer stage and histology prediction using small data samples. *Physica Medica, 90*, 13–22. https://doi.org/10.1016/j.ejmp.2021.08.015
31. Moon, W. K., Lee, Y. W., Huang, Y. S., Lee, S. H., Bae, M. S., Yi, A., Huang, C. S., & Chang, R. F. (2017). Computer-aided prediction of axillary lymph node status in breast cancer using tumor surrounding tissue features in ultrasound images. *Computer Methods and Programs in Biomedicine, 146*, 143–150. https://doi.org/10.1016/j.cmpb.2017.06.001
32. Wu, H., Patel, R. B., Zheng, Y., Solorio, L., Krupka, T. M., Ziats, N. P., et al. (2012). Differentiation of benign periablational enhancement from residual tumor following radio-frequency ablation using contrast-enhanced ultrasonography in a rat subcutaneous colon cancer model. *Ultrasound in Medicine and Biology, 38*, 443–453. https://doi.org/10.1016/j.ultrasmedbio.2011.12.008
33. Wu, H., Exner, A. A., Krupka, T. M., Weinberg, B. D., Patel, R., & Haaga, J. R. (2009). Radiofrequency ablation: post-ablation assessment using CT perfusion with pharmacological modulation in a rat subcutaneous tumor model. *Academic radiology, 16*, 321–331. https://doi.org/10.1016/j.acra.2008.09.008
34. Wei, J., Jiang, H., Gu, D., Niu, M., Fu, F., Han, Y., Song, B., & Tian, J. (2020). Radiomics in liver diseases: Current progress and future opportunities. *Liver International, 40*, 2050–2063. https://doi.org/10.1111/liv.14555
35. Han, H., Jin, Y., Liu, R., Ji, Z. F. Z., & Wang, W. (2022). Early differentiation of residual tumor and inflammation rim after ablation of rabbit VX2 liver tumor by quantitative analysis of contrast-enhanced ultrasound. *Fudan University Journal of Medical*, *49*(01), 44–49. https://doi.org/10.3969/j.issn.1672-8467.2022.01.006.
36. Kan, X., Zhang, Y., Zheng, C., Li, L., Chen, J., Wu, Y., Guo, T., & Xiong, B. (2016). Stress test of contrast-enhanced US with Phenylephrine in a rabbit VX2 liver tumor model: Differentiating benign periablational enhancement from residual tumor after radiofrequency ablation. *Journal of Vascular and Interventional Radiology, 27*, 1077–1085. https://doi.org/10.1016/j.jvir.2016.02.012